Two-frequency parametric excitation of surface waves

Thomas Besson and W. Stuart Edwards
Department of Physics, Haverford College, Haverford, Pennsylvania 19041

Laurette S. Tuckerman*
Laboratoire d'Informatique pour la Mécanique et les Sciences de l'Ingenieur (CNRS), Boite Postale 133, 91403 Orsay Cedex, France
(Received 30 November 1995)

Threshold accelerations necessary to excite surface waves parametrically in a vertically vibrated fluid layer are presented and compared with a linear stability analysis of the full hydrodynamic equations. The effects of viscosity and finite depth are treated rigorously. The case of two-frequency forcing is considered in detail because of its relevance to recently reported pattern forming phenomena. Absolute agreement between theory and experiment, generally to within 2%, is obtained for kinematic viscosities in the range 10–50 cS (1 S=1 cm^2/s) and three frequency ratios. A slight discrepancy is noted for single-frequency forcing at high frequencies. [S1063-651X(96)07807-5]

PACS number(s): 47.35.+i, 47.20.Ky

I. INTRODUCTION

The Faraday instability, produced by vertical oscillation of an incompressible liquid with a free upper surface, provides an excellent context in which to explore a variety of issues related to nonlinear pattern formation. Many of the regular patterns that are possible in two dimensions can be produced in this system for suitable choices of parameters, including one-dimensional standing waves (''stripes''), squares, hexagons, and triangles. Octagonal and dodecagonal quasicrystalline patterns (''quasipatterns''), which lack strict translational periodicity, have also recently been reported [1–4]. In addition, the formation and propagation of defects in these patterns can be easily studied, as can the development of spatiotemporally chaotic patterns (for a review, see [5]).

Some of these patterns, including the hexagonal and dodecagonal patterns shown in Fig. 1, are most readily produced by generalizing the conventional sinusoidal forcing to a mixture of two frequencies. An explanation for this effect in terms of the breaking of the subharmonic symmetry of the induced waves was given by Edwards and Fauve [4]. However, to develop a more complete theory of the quasipatterns, it is desirable to have a quantitative understanding of the linear stability problem with multiple frequency forcing, which is the subject of this paper. We note that Müller's observation of regular triangles [6] also resulted from two-frequency forcing.

We first extend the stability analysis of Kumar and Tuckerman [7] to the case of two-frequency forcing. The effects of viscosity and finite depth are treated exactly for layers of infinite lateral extent. We then describe a set of precise experiments yielding quantitative tests of the two-frequency theory to within 2% (for stability thresholds) for three fluids with kinematic viscosities ν in the range 10–50 cS (1 cS $=0.01$ cm^2/s). We also test the stability theory for single-frequency forcing more precisely than measurements previously reported. Since the effects of viscous damping are subtle, the improved precision is important to a quantitative understanding.

For single-frequency forcing, there is substantial literature. We refer the reader to [8] for a review and bibliography of previous theoretical and experimental work. (Our experimental results will be compared to those of Ref. [8] in Sec. V.) A two-frequency stability calculation was also recently performed by Beyer and Friedrich [9]. No precise experimental tests on two-frequency forcing have been previously reported.

In contrast to low-viscosity, large-depth experiments such as [2] and references therein and experiments at low aspect ratio (for a general review see [10]), our study is concerned with the case of a large aspect ratio, finite depth, and finite viscosity.

II. THEORETICAL CONSIDERATIONS

We consider the linear stability of the interface between two incompressible Newtonian fluids $j=1,2$. The lower fluid $j=1$ is a liquid layer of finite depth h. The upper layer $j=2$ is air, of small but nonzero density, extending upward to $z=\infty$. The hydrodynamic problem and the numerical method for its solution are discussed at some length in [7]; here we summarize the main points.

Elimination of the pressure in the linearized Navier-Stokes equations leads to

$$(\partial_t-\nu_j\nabla^2)\nabla^2 w_j=0, \tag{2.1}$$

where $w_j(x,y,z,t)$ and ν_j are the vertical velocity and kinematic viscosity, respectively, in each fluid layer $j=1,2$. In a reference frame that oscillates vertically with the container and whose origin $z=0$ coincides with the flat interface, the boundary conditions are

$$w_j=\partial_z w_j=0 \quad \text{at } z=-h,\infty. \tag{2.2}$$

The interface position is $z=\zeta(x,y,t)$ and is advected by the fluid

$$\partial_t\zeta=w. \tag{2.3}$$

(Horizontal advection is nonlinear and is therefore omitted.)

*Electronic address: laurette@limsi.fr

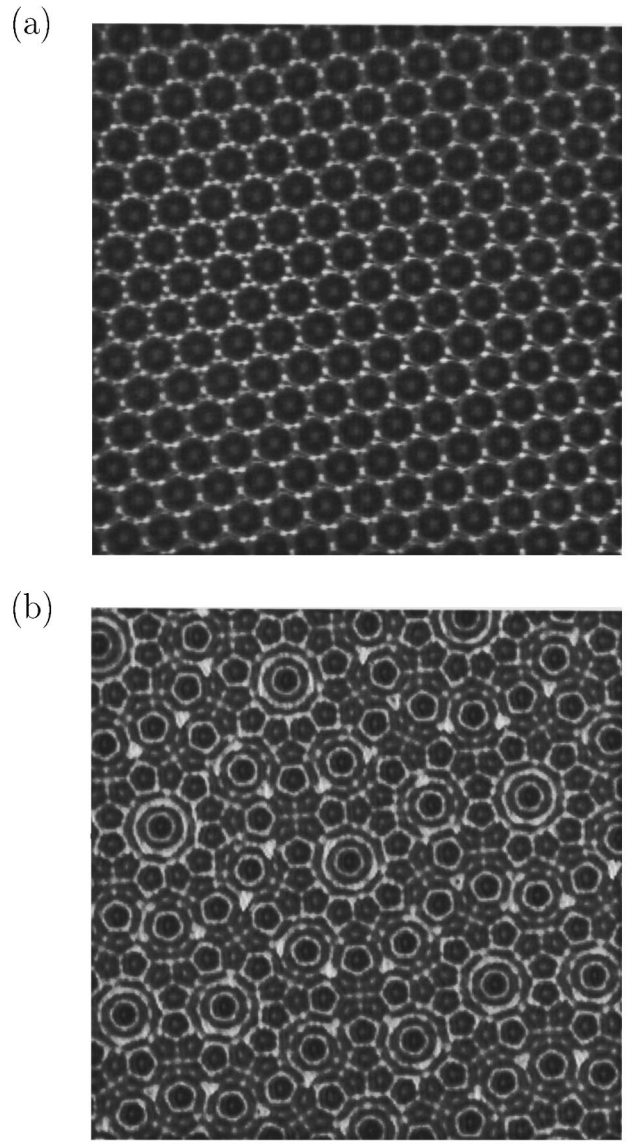

FIG. 1. (a) Hexagonal and (b) dodecagonal patterns produced somewhat beyond the critical acceleration for two-frequency forcing. Parameter values leading to these states are given in Ref. [4].

Several conditions must be imposed at the interface. Continuity of velocity and of tangential stress imply that

$$\Delta w = \Delta \partial_z w = 0, \tag{2.4a}$$

$$\Delta \rho \nu (\nabla_H^2 - \partial_{zz}) w = 0, \tag{2.4b}$$

where ∇_H^2 is the horizontal Laplacian, ρ is the density, and Δ denotes the difference in the given quantity across the interface (e.g., $\Delta \rho \nu \partial_{zz} w \equiv \rho_2 \nu_2 \partial_{zz} w_2|_{z=\zeta} - \rho_1 \nu_1 \partial_{zz} w_1|_{z=\zeta}$).

Curvature of the interface yields a normal stress discontinuity of $-\sigma \nabla_H^2 \zeta$, where σ is the surface tension. The total balance of forces normal to the interface is

$$\Delta \rho [\partial_t - \nu(3\nabla_H^2 + \partial_{zz})] \partial_z w = \Delta \rho [g + f(t)] \nabla_H^2 \zeta + \sigma \nabla_H^4 \zeta, \tag{2.4c}$$

where $g \equiv 980.665$ cm/s^2 is the usual gravitational acceleration and $f(t)$ is its effective modulation by the imposed vertical oscillation. [Although the full hydrodynamic problem would require the interface conditions (2.4a)–(2.4c) to be applied at $z = \zeta(x,y,t)$, linearization justifies the more tractable use of $z = 0$.]

The linear system (2.1–2.4) is homogeneous in the horizontal directions and periodic in time. With the assumption of boundedness (as $x,y \to \pm\infty$), the solutions are of the Floquet-Fourier form

$$w_j(x,y,z,t) = \sin(k_x x + k_y y) e^{(\mu + i\alpha)t} \sum_n w_{jn}(z) e^{in\omega t} + \text{c.c.}, \tag{2.5a}$$

$$\zeta(x,y,t) = \sin(k_x x + k_y y) e^{(\mu + i\alpha)t} \sum_n \zeta_n e^{in\omega t} + \text{c.c.}, \tag{2.5b}$$

where $2\pi/\omega$ is the period of the vertical acceleration $f(t)$, $k = \sqrt{k_x^2 + k_y^2}$ is the horizontal wave number, and $\mu + i\alpha$ is the Floquet exponent, with $0 \leqslant \alpha \leqslant \omega/2$. The z dependence of w is determined by substituting (2.5a) into (2.1):

$$w_{jn}(z) = a_{jn} e^{kz} + b_{jn} e^{-kz} + c_{jn} e^{q_{jn} z} + d_{jn} e^{-q_{jn} z}, \tag{2.6a}$$

where

$$q_{jn}^2 \equiv k^2 + \frac{\mu + i(\alpha + n\omega)}{\nu_j}. \tag{2.6b}$$

Equations (2.2) and (2.3), which do not couple the different temporal Fourier components, allow the four coefficients in (2.6a) to be expressed in terms of ζ_n.

The remaining equation (2.4c) can then be written as

$$A_n \zeta_n = 2[f\zeta]_n, \tag{2.7}$$

where A_n is an algebraic function of the physical parameters and μ, α, k and $[f\zeta]_n$ is the nth Fourier component of the product of $f(t)$ and $\Sigma_{n'} \zeta_{n'} e^{in'\omega t}$. With the two-frequency vertical acceleration given by

$$f(t) = a[\cos(\chi)\cos(m\omega t) + \sin(\chi)\cos(l\omega t + \phi)], \tag{2.8}$$

we have

$$[f\zeta]_n = \frac{a}{2} [\cos(\chi)(\zeta_{n-m} + \zeta_{n+m}) + \sin(\chi)(e^{i\phi}\zeta_{n-l} + e^{-i\phi}\zeta_{n+l})], \tag{2.9}$$

with appropriate modifications to ensure that ζ is real and is represented by a truncated Fourier series in (2.5b). Equation (2.7) can therefore be written as

$$\mathcal{A}\hat{\zeta} = a\mathcal{B}\hat{\zeta}, \tag{2.10}$$

where $\hat{\zeta}$ is the vector of temporal Fourier coefficients ζ_n, $\mathcal{A}$ is the diagonal matrix of A_n, and $\mathcal{B}$ is a banded matrix containing (in the present case of two-frequency forcing) four super- and subdiagonals. [Beyer and Friedrich [9] derive an equation equivalent to (2.10), using an integro-differential equation for ζ.] With $\mathcal{A}$ or $\mathcal{B}$ invertible, Eq. (2.10) constitutes

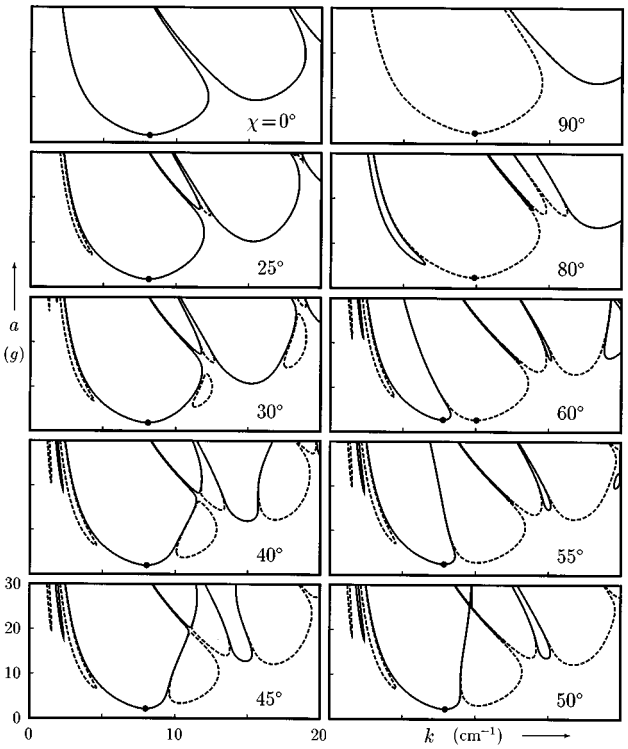

FIG. 2. Stability tongues for a 20-cS fluid (PS039.5 of Table I) layer of depth $h=0.3$ cm for two-frequency forcing of the form $f(t)=a[\cos(\chi)\cos(m\omega t)+\sin(\chi)\cos(l\omega t+\phi)]$, with $(m,l)=(4,5)$, $4\omega/2\pi=44$ Hz, and $\phi=0°$. Solid (dashed) curves correspond to a temporal response that is harmonic (subharmonic) with respect to the period $2\pi/\omega$. Dots represent critical wave numbers and amplitudes. The amplitude mixing angle $\chi=0°$ corresponds to pure 4ω forcing. At $\chi=25°$, another system of narrow tongues has descended from high a. Intermediate values $\chi=30°,40°,45°,50°,55°$ depict a complicated process involving the appearance of ''islands'' and their growth into tongues. At the bicritical value $\chi=60°$, two wave numbers $k_-=10.05$ cm^{-1} and $k_+=7.76$ cm^{-1} share the same critical amplitude $a=2.70g$. At $\chi=80°$, narrow tongues retreat to high a. The value $\chi=90°$ corresponds to pure 5ω forcing.

an eigenvalue problem for the forcing amplitude a and can be solved by calling a standard subroutine, in this case RG from EISPACK. At most 20 temporal Fourier coefficients suffice to resolve $\hat{\zeta}$ for typical calculations such as $(m,l)=(4,5)$ and $a\leqslant 30g$.

With fixed physical parameters, the solution of (2.10) yields a set of amplitudes a that depend on μ, α, and k. To obtain marginal stability curves, we fix k and α, set the growth rate μ to 0, and select the smallest real positive a obtained. We find that setting the imaginary part α of the Floquet exponent to any value other than 0 and $\omega/2$ yields only physically unrealizable complex values of a, indicating that the time dependence of the marginal modes is always either harmonic ($\alpha=0$) or subharmonic ($\alpha=\omega/2$). (We have not determined rigorously that this is true in all cases.)

Figure 2 presents marginal stability curves in the (k,a) plane for selected values of the mixing angle χ of (2.8) with $(m,l)=(4,5)$. The curves delineate tongues, inside of which the growth rate μ is positive. We wish to understand how the structure of these tongues evolves as χ varies from 0° to 90°, i.e., as one interpolates between pure 4ω and pure 5ω forcing.

To understand Fig. 2, it is helpful to recall the undamped, single-frequency case, in which the equation governing the interface between two ideal fluids forced at the single angular frequency ω reduces to the classic undamped Mathieu equation [11]. One finds tongues in the (k,a) plane extending down to $a=0$. As $a\to 0$, the temporal response within each tongue approaches $\zeta\sim\cos[(n/2)\omega t]$, where $n=1,2,\ldots$ indexes the tongues as k increases. Thus subharmonic (n odd) tongues alternate with harmonic (n even) tongues. For a finite, ζ contains a mixture of frequencies that are either all odd multiples of $\omega/2$, for a subharmonic tongue, or all even, for a harmonic tongue. The tongues widen with a, the boundary of one tongue becoming nearly tangent to that of the next as $a\to\infty$.

For fixed values of (k,a), there are only two Floquet exponents, and their sum is zero because the system is nondissipative. On the tongue boundaries, the real part μ and the imaginary part α of both Floquet exponents vanish. Inside the tongues, the exponents are real and of equal magnitude and opposite sign, whereas outside the tongues, the two exponents form a complex conjugate imaginary pair. This is best understood in terms of the Floquet multipliers, defined as $\exp[(\mu+i\alpha)(2\pi/\omega)]$, which are real or a complex conjugate pair and whose product is one. Let us consider the behavior of the multipliers for some fixed finite a as k is varied. As a subharmonic tongue is encountered, the multipliers, both initially -1, travel in opposite directions along the real axis, but eventually reverse directions to meet again at -1 as the tongue is exited. Between tongues, the multipliers become complex and travel in opposite directions along the unit circle, coalescing at $+1$ when a harmonic tongue is entered. They travel in opposite directions along the real axis as the harmonic tongue is traversed, returning to $+1$ as the tongue is exited. They then travel along the unit circle to -1, where a new subharmonic tongue is entered and the whole process repeats.

With the inclusion of viscosity in the hydrodynamic equations or of damping in the Mathieu equation, the tongues become rounded, as can be seen in Fig. 2, or in more detail in [7] and in [8]. Their minima are no longer at $a=0$; the lowest minimum defines the critical amplitude and wave number. The critical tongue is usually that corresponding to the lowest k and is subharmonic. (An exception to this rule has recently been discovered by Kumar [12] for very shallow or very viscous fluid layers.) Damping decreases $\mu(k,a)$ so that the curves on which the Floquet multipliers become complex no longer coincide with the tongue boundaries, but are located outside the tongues, where $\mu<0$, as can be seen in [9]. For the hydrodynamic problem, there is a countable infinity of Floquet multipliers for each (k,a) pair.

Returning to Fig. 2, the case $\chi=0$ shows the instability tongues for a viscous ($\nu=20$ cS) fluid layer forced at the single frequency 4ω. The tongues can be labeled as corresponding roughly to $2\omega,4\omega,\ldots$ (their temporal responses would approach these pure frequencies as ν was decreased). Thus, although the tongues follow the classic alternation between subharmonic and harmonic with respect to the period $2\pi/4\omega$, they are all harmonic with respect to the period $2\pi/\omega$ of the two-frequency functional form (2.8). The critical wave number is $k_+=8.15$ cm^{-1} and the critical amplitude $a_+=1.62g$.

Increasing χ corresponds to adding an increasing component of $\cos(5\omega t+\phi)$ in the forcing function (2.8). New sets of three narrow tongues—subharmonic, harmonic, and subharmonic—descend from high a, between each pair of the original (harmonic) single-frequency tongues, as seen for $\chi=25°$. Some of the tongues are so narrow that they cannot be seen on the scale of Fig. 2. As a general guide, harmonic and subharmonic tongues alternate—a structure inherited from the single-frequency case—but only for sufficiently high a.

The sequence of χ values from 30° to 55° depicts a curious and complicated phenomenon. New $\mu=0$ curves appear, but the regions they delineate cannot all be classified as tongues, since they do not extend to arbitrarily high a. Instead, some are ''islands'' that occupy a finite range of a. One prominent island is adjacent to the largest harmonic tongue and is itself subharmonic. This island widens in k and elongates in a as χ is further increased, eventually merging with a subharmonic tongue that exists at higher a. By $\chi=59.5°$, the island turned tongue has a minimum whose amplitude coincides with that of the harmonic tongue. This is the bicritical point at which $a_+=a_-=2.70g$; the corresponding critical wave numbers are $k_+=7.76\ \mathrm{cm}^{-1}$ and $k_-=10.05\ \mathrm{cm}^{-1}$.

The value $\chi=80°$ shows the reversal of the phenomenon seen for χ near 0: sets of very narrow tongues retreat to high a. At $\chi=90°$ there remains the regular alternating sequence of subharmonic and harmonic tongues corresponding to forcing at the pure frequency 5ω, with $k_-=9.86\ \mathrm{cm}^{-1}$ and $a_-=2.32g$.

III. EXPERIMENTAL APPARATUS AND METHODS

A. Mechanical system and fluids

The apparatus is shown in Fig. 3. A circular container filled with a thin layer of silicone oil is mechanically coupled to a computer controlled electromagnetic vibrator and the induced wave patterns are visualized by reflected light. This system has several unique features: large aspect ratio (more than 100 wavelengths); high achievable accelerations (up to $15g$); precise computer control of the exciting wave form, including the amplitudes and the relative phases of the various frequency components; and automated determination of stability boundaries. A detailed description follows.

Silicone oils were used for these experiments because of their relatively low surface tension, which yields high wave numbers at a given frequency; and stable viscosity and surface tension over long periods of time. In comparison to water, surface contamination is not a problem. Viscosities are determined using a falling ball viscometer to an accuracy of $\pm 2\%$. The density and surface tension are provided by the manufacturer to an accuracy of better than $\pm 1\%$. The various fluid parameters are shown in Table I.

The diameter of the fluid container (32 cm) is sufficient to achieve aspect ratios (diameter to wavelength) up to 100. It is machined from a solid piece of aluminum 1.4 cm thick that is bolted to a Delrin temperature control plate. This container assembly is attached to an electromagnetic vibrator (Vibration Test Systems VTS-500) that generates peak forces up to 2200 N. The maximum acceleration ($21g$) is determined by the mass (10.7 kg) of the container assembly; sustained operation is possible only to $15g$ due to overheating of the power amplifier. Flexing of the container is eliminated by its thickness and conical shape and by the structure of the brace and the use of two bolt circles. Though the container is rigid, there remains some inhomogeneity of acceleration (about 2–5 % across the surface of the container) due to horizontal motion within the vibrator.

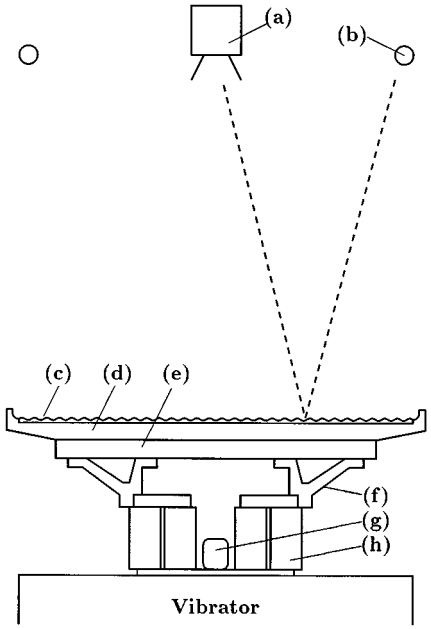

FIG. 3. Apparatus and visualization. (a) Camera. (b) Circular ring of 58 incandescent lights. (c) Silicone oil fluid layer, 0.3 cm deep. (d) Anodized aluminum container, 32 cm diameter, 1.4 cm thick. (e) Temperature control plate. (f) Aluminum brace. (g) Piezoelectric accelerometer. (h) Standoffs, 1 in. diameter, mounted on vibrator; four of eight are shown.

The container is designed to minimize the formation of meniscus waves by filling the fluid to the top of a ledge machined into the sidewall (cf. Refs. [13,14,8]). The depth of the fluid layer is 0.3 cm in all cases. The fluid is maintained at 25.0($\pm$0.1) °C by circulating bath water through the temperature control plate. The container is enclosed in a glass and Plexiglas box to prevent contamination of the surface.

B. Wave-form generation and control

The vibrator is driven in real time by a computer generated wave form composed of two frequencies

TABLE I. Fluid parameters. Experimental working fluids are commercial silicone oils (products of United Chemical Technologies) at 25 °C. Viscosity values are obtained from falling-ball viscometer measurements. Density and surface tension values are the manufacturer's specifications.

Product	ν (cS)	σ (dyn/cm)	ρ (g/cm^3)
PS039	10.04$\pm$0.3	20.1	0.935
PS039.5	20.9 $\pm$0.5	20.6	0.950
PS040	51.9 $\pm$1.3	20.8	0.960
PS041	98.9 $\pm$1.3	20.9	0.966

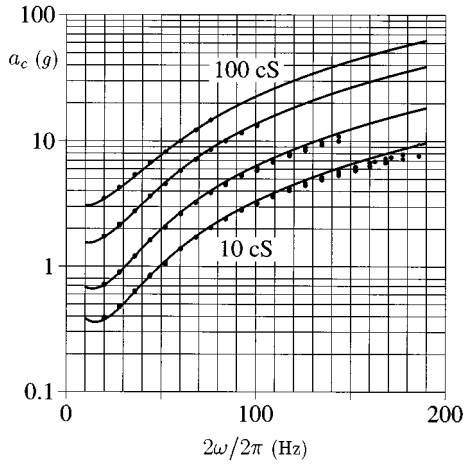

FIG. 4. Stability boundaries for single-frequency forcing. Four sets of theoretical (solid lines) and experimental (dots) results are shown for the four kinematic viscosities 10, 20, 50, and 100 cS. (See Table I.) Multiple experimental data sets are superposed. Quantitative agreement is excellent at low frequencies. A discrepancy is apparent for frequencies above about 120 Hz.

$$f(t)=a[\cos(\chi)\cos(m\omega t)+\sin(\chi)\cos(l\omega t+\phi)], \tag{3.1}$$

where χ is known as the mixing angle. This wave form is converted to an analog signal (by a National Instruments AT-MIO-16X interface board) and is amplified by a Vibration Test Systems PA1200 power amplifier that drives the electromagnetic vibrator. The resulting acceleration is measured simultaneously using a piezoelectric accelerometer (Wilcoxon 726T), whose output is Fourier analyzed by the computer. The amplitudes and phases of the two spectral components of the accelerometer signal are compared to those in the desired wave form and the driving wave form is updated approximately once per second. The control is linear in the sense that each spectral component is updated on the basis of the measured amplitude and phase of that component. The feedback removes amplitude and phase errors due to the power amplifier and vibrator. Residual fluctuations in the acceleration are about $\pm 0.002g$ (about 0.1% typically). The accelerometer was independently calibrated to $\pm 0.5\%$ using optical interferometry.

C. Visualization

Patterns are visualized by reflecting light from the surface of the fluid. The light originates from an annulus (inner radius $R_i = 47$ cm, outer radius $R_o = 52$ cm) of 58 incandescent flashlight bulbs (see Fig. 3). Since the annulus produces axisymmetric lighting, this visualization technique does not favor any direction in the pattern. The distance between the camera, located at the center of the annulus, and the container is $L = 3.40$ m. Finite surface slopes (in the range $4.2° \pm 0.2°$) reflect light to the camera. The anodized aluminum container provides a black background.

The 512×512 square-pixel charge coupled device camera (Dalsa CA-D2-0512) is equipped with a ferroelectric liquid crystal shutter (Displaytech VS2200). It is interfaced to the computer via a fast frame-grabber card (Bitflow Data Raptor). Shutter timing is synchronized with the wave-form generation. Typically, the exposure time is one full period of the forcing; shorter exposures (down to 1 ms) are also used.

D. Threshold measurement procedure

The measurement of stability thresholds is performed automatically by the controlling computer. The protocol is to fix all parameters expect the overall acceleration amplitude a of (3.1). As the acceleration is increased to destabilize the flat surface, the computer monitors the video image, measuring the intensity of light reflected from the fluid surface at the center of the container. If a change of light intensity is observed in a $(0.4\text{-cm})^2$ region (i.e., if a pattern has formed), the acceleration is recorded and the independent variable, either the mixing angle (for two-frequency measurements) or the frequency (for single-frequency measurements) is incremented. Otherwise, the acceleration is increased by $0.002g$ and the reflected light intensity is measured again after approximately 15 s. This interval is sufficient to eliminate threshold errors due to instability delay to within 0.1%.

IV. EXPERIMENTAL RESULTS

A. Sources of error

The most important source of uncertainty in the experimental parameters is related to the viscosity, which was measured to within $\pm 2\%$. Using the linear stability analysis and numerical code of Sec. II, we found that a 1% variation in viscosity results approximately in a 1% variation in the computed threshold. Uncertainty in the surface tension and density does not contribute significantly to uncertainty in computed threshold.

Inhomogeneity of vibration combined with the subcritical nature of the instability can result in underestimation of the true linear stability threshold, as we now explain. The pattern typically forms on one side of the container because of the 2–5 % inhomogeneity of vibration and grows towards the opposite edge as the forcing acceleration is increased. Furthermore, as observed by Edwards and Fauve [4], a hysteresis band exists for $38° \leqslant \chi \leqslant 70°$ for two-frequency forcing. At the bicritical point, depending on the nature of the forcing, the width of the hysteresis band can be as large as 5%. The combination of these factors causes the computer to record thresholds that are low by approximately 1–2.5 %. (That is, the detected pattern is actually due to an instability at a different location, where the excitation amplitude is larger.) Data points for which hysteresis causes the pattern to grow all the way to the center immediately after a pattern has formed at the edge of the container are denoted by triangles in Figs. 5–7.

A systematic error in threshold measurement could result from the finite surface slope necessary to reflect light into the camera. However, we checked by direct observation and found that this error is less 0.1% in all cases.

Accelerations measured by the accelerometer attached to the vibrator (see Fig. 3) were found to be systematically higher, by 0.4–0.9 %, than that at the center of the vibrating cell. All measurements were corrected for this error.

B. Results

Threshold measurements for single-frequency forcing are shown in Fig. 4 for various viscosities. The theoretical

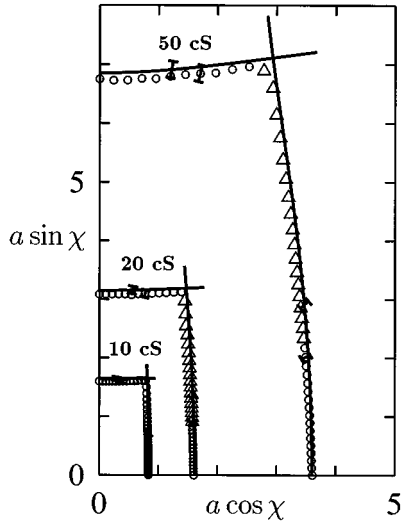

FIG. 5. Stability boundaries for forcing with two frequencies $(2\omega,3\omega)$ and phase angle $\phi=0°$. Here $a\cos(\chi)$ and $a\sin(\chi)$ are the acceleration amplitudes at $2\omega,3\omega$, respectively. $(2\omega/2\pi=44$ Hz; $\nu=10$, 20, and 50 cS.) Solid lines are theoretical predictions. Circles and triangles are experimental data. The $\pm 2\%$ error bar on the theoretical predictions is due to the 2% accuracy of our viscosity measurements. The $\pm 2\%$ error bar on the experimental data is an accumulation of errors explained in the text. Triangles denote experimental data points that are affected by the existence of hysteresis as described in Sec. IV A.

curves were obtained using the numerical code of Sec. II and Ref. [7]; there are no adjustable parameters. To show the degree of reproducibility of the experimental measurements, multiple data runs are shown.

Threshold measurements for two-frequency forcing are shown in Figs. 5, 6, and 7 for the frequency pairs $(2\omega,3\omega)$, $(4\omega,5\omega)$, and $(6\omega,7\omega)$, respectively. All use the lower ''base'' frequency $m\omega/2\pi\equiv 44$ Hz. The horizontal and vertical coordinate axes correspond to the amplitudes of the imposed accelerations at the lower and higher frequencies, respectively. The theoretical curves are the critical amplitudes obtained using the Kumar-Tuckerman code. (The 20-cS theoretical curves of Fig. 6 are the tongue minima whose evolution was presented in detail in Fig. 2.) Each experimental data point shown corresponds to the average of three independent measurements and is reproducible to approximately 0.5%.

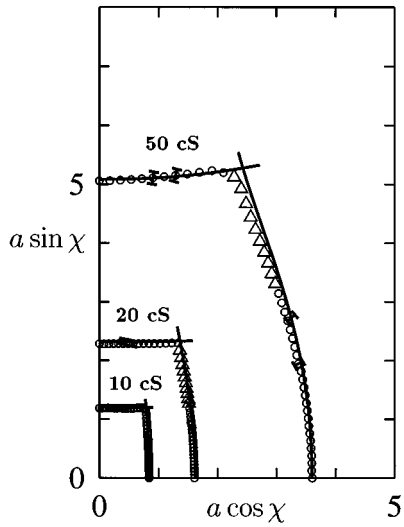

FIG. 6. Stability boundaries for $(4\omega,5\omega)$ forcing, $4\omega/2\pi=44$ Hz, $\phi=0°$. Symbols are the same as in Fig. 5. The 20-cS theoretical curves are the tongue minima shown in Fig. 2.

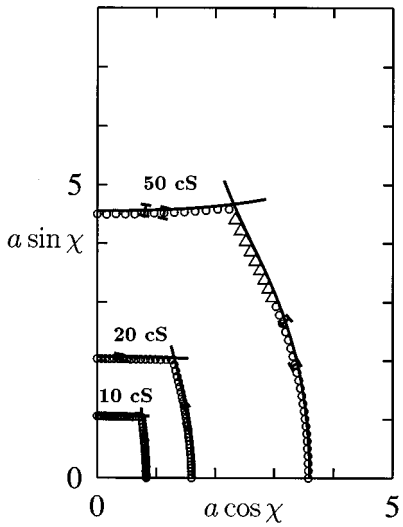

FIG. 7. Stability boundaries for $(6\omega,7\omega)$ forcing, $6\omega/2\pi=44$ Hz, $\phi=0°$. Symbols are the same as in Fig. 5.

V. DISCUSSION AND CONCLUSIONS

For single-frequency forcing, we find quantitative agreement with the theoretical calculations to within about 2%, except at frequencies above about 120 Hz. We emphasize that there are no adjustable parameters. Our results extend those of Bechhoefer *et al.* [8] in the following respects: (a) the large aspect ratio of the present experiments allows lateral boundaries to be neglected to within the stated precision; (b) our measurements include fluids with different viscosities; (c) the measurements are extended to somewhat higher frequencies. For high frequencies, the theory overestimates the threshold by about 5%.

We speculate that the discrepancy at high frequencies could result from physical effects that are not included in the hydrodynamic description, for example, surface viscosity, compressibility, or viscoelastic effects. It is also possible that the numerical method fails to accurately solve the linear eigenproblem when the values of q_{jn} in Eq. (2.6) are such that $q_{jn}h \gg 1$, even though $kh \sim 1$. This is true for all n when $\omega/(\nu/h^2)$ is large. Physically, the wave number q_{11} is associated with boundary layers at the interface and on the container bottom, which can be much thinner than the fluid depth h. The discrepancy could also be due to mechanical imperfections of the experiment.

For two-frequency forcing at $m\omega/2\pi=44$ Hz, we find excellent agreement for the entire stability boundary. Our results establish that for a finite-depth viscous layer, linear theory (including damping due to bulk viscosity, the boundary layer at the container bottom, and the shear layer at the

free surface) correctly predicts critical accelerations to experimental accuracy. Thus we are justified in ignoring sidewall boundaries. Also, effects due to possible contamination of the surface do not seem to be significant. Therefore, at least for low to moderate frequencies, all of the important physics is included in the stability calculations and subsequent efforts to understand the exotic patterns above onset can proceed from a firm foundation, at least for low to moderate frequencies.

ACKNOWLEDGMENTS

We would like to acknowledge helpful discussions with Jerry Gollub, Benoit Pier, Douglas P. Vallette, and Eric Bosch. Bruce Boyes provided excellent technical support. This work is supported by the National Science Foundation under Grant No. DMR-9319973. L.S.T. benefitted from support by the Fondation Scientifique of the Région Rhône-Alpes during an initial phase of this work at the Ecole Normale Supérieur de Lyon.

[1] B. Christiansen, P. Alstrom, and M. Levinsen, Phys. Rev. Lett. **68**, 2157 (1992).
[2] B. Christiansen, P. Alstrom, and M. T. Levinsen, J. Fluid Mech. **291**, 323 (1995).
[3] W. Edwards and S. Fauve, Phys. Rev. E **47**, R788 (1993).
[4] W. Edwards and S. Fauve, J. Fluid Mech. **278**, 123 (1994).
[5] M. Cross and P. Hohenberg, Rev. Mod. Phys. **65**, 851 (1993).
[6] H. Müller, Phys. Rev. Lett. **71**, 3287 (1993).
[7] K. Kumar and L. S. Tuckerman, J. Fluid Mech. **279**, 49 (1994).
[8] J. Bechhoefer, V. Ego, S. Manneville, and B. Johnson, J. Fluid Mech. **288**, 325 (1995).
[9] J. Beyer and R. Friedrich, Phys. Rev. E **51**, 1162 (1995).
[10] J. Miles and D. Henderson, Annu. Rev. Fluid Mech. **22**, 143 (1990).
[11] T. Benjamin and F. Ursell, Proc. R. Soc. London Ser. A **225**, 505 (1954).
[12] K. Kumar, Proc. R. Soc. London Ser. A **452**, 1113 (1996).
[13] T. Benjamin and C. Scott, J. Fluid Mech. **2**, 241 (1979).
[14] S. Douady, J. Fluid Mech. **221**, 383 (1990).